World Academy of Science, Engineering and Technology
International Journal of Mechanical and Mechatronics Engineering
Vol:7, No:7, 2013

Multi-Objective Optimization of a Steam Turbine Stage

Alvise Pellegrini and Ernesto Benini

***Abstract*—**The design of a steam turbine is a very complex engineering operation that can be simplified and improved thanks to computer-aided multi-objective optimization. This process makes use of existing optimization algorithms and losses correlations to identify those geometries that deliver the best balance of performance (i.e. Pareto-optimal points).

This paper deals with a one-dimensional multi-objective and multi-point optimization of a single-stage steam turbine. Using a genetic optimization algorithm and an algebraic one-dimensional ideal gas-path model based on loss and deviation correlations, a code capable of performing the optimization of a predefined steam turbine stage was developed. More specifically, during this study the parameters modified (i.e. decision variables) to identify the best performing geometries were solidity and angles both for stator and rotor cascades, while the objective functions to maximize were total-to-static efficiency and specific work done.

Finally, an accurate analysis of the obtained results was carried out.

***Keywords*—**Steam turbine, optimization, genetic algorithms.

NOMENCLATURE

c	Absolute flow velocity
h	Enthalpy
L	Specific turbine stage work
T	Temperature
u	Turbine rotor peripheral velocity
w	Relative flow velocity

Greek symbols

α_{1c}	Outlet stator blade angle
β_{1c}	Inlet rotor blade angle
β_{2c}	Outlet rotor blade angle
η_{ts}	Total-to-static stage efficiency
σ_R	Rotor cascade solidity
σ_S	Stator cascade solidity
ε_R	Rotor flow deflection

Subscript

0	Upstream of stator cascade
1	Downstream of stator cascade
2	Downstream of rotor cascade
is	Isentropic
m	Axial component
R	Rotor
S	Stator
u	Tangential component

Superscript

0	Total quantity

A. Pellegrini and E. Benini are with the Department of Industrial Engineering, University of Padova, Via Venezia, 1 – 35131 Padova, Italy.

I. INTRODUCTION

TRADITIONAL approaches for turbine design are based either on simplified theoretical correlations or on empirical models built on collected data sets. Both of these methods suggest suitable ranges for the most relevant design parameters but rarely indicate the *best* solutions.

To overcome these limitations, optimization algorithms are today widely adopted which allow automatically evaluating and comparing performance of many different solutions, thus leading to a real multi-objective design approach [1]. Multi-point methods are also becoming quite popular among researchers and engineers as they make it possible to optimize a design considering more than one operating conditions.

In the present paper, a one-dimensional multi-objective and multi-point optimization of a single-stage steam turbine is proposed. To reach this goal, an optimization algorithm and an algebraic one-dimensional, ideal gas-path, model based on loss and deviation correlations are coupled together. Design parameters are turbine cascade solidity and blade angles, both for stator and rotor cascades, while the objective functions to maximize are total-to-static efficiency and specific work done.

II. LOSS CORRELATION FOR PERFORMANCE PREDICTION

Loss and deviation correlations are today widely used by turbines manufacturers in view of their capability to give reasonable on/off performance predictions. Such an approach is still recognized as the only viable to obtain rapid responses and is currently used for multiple scopes among which design and preliminary optimization of the operative fluid path.

Several loss formulations are available in the open literature which make use of both algebraic models and look-up tables (based on empirical data) to calculate turbine stage performance using a mean line approach. However, since no definitive indications about their correct usage are available, the choice of loss formulation to use in this work was made on the bases of indications given in [2]. In this paper, the Craig & Cox performance prediction model, fully described in [4], [5], was used. Moreover, to evaluate tip leakage losses, not considered by Craig & Cox model, Ainley & Mathieson correlations were adopted [3].

As the entire optimization program was written in MATLAB language, the source code for Craig & Cox model

was an arranged version of the one used and tested in [2].

III. Code Implementation and Baseline Geometry

A. Decision Variables and Objective Function

Initially, code implementation required interfacing of MATLAB optimization function *gamultiobj* with Craig & Cox model. To complete this operation, objective functions and decision variables had to be established.

As suggested by Craig & Cox model, decision variables were chosen among those having more influence on turbine performance. This led to define the following design variables:

- Outlet stator blade angle α_{1c};
- Stator cascade solidity σ_S;
- Inlet rotor blade angle β_{1c};
- Outlet rotor blade angle β_{2c};
- Rotor cascade solidity σ_R.

Among them, cascade solidities influence mainly deviation angle, wall friction losses, and stall behavior, while blade angles influence mainly stator-rotor interaction, stall behavior, and rotor outflow conditions.

Objective functions to maximize were defined as:

- Specific turbine stage work $L = h_0^0 - h_2^0$;
- Total-to-static stage efficiency $\eta_{ts} = \dfrac{h_0^0 - h_2^0}{h_0^0 - h_{2,is}}$.

A crucial aspect of the problem was that the objective functions chosen were conflicting targets; in fact, assuming u as a constant, specific work can be expressed as:

$$L = u \cdot (c_{u1} - c_{u2}) = u \cdot (w_{u1} - w_{u2}) \propto \varepsilon_R \qquad (1)$$

However, as confirmed by Craig & Cox losses correlations, a high deflection (ε_R) is associated with high profile losses and high secondary losses: this means that an increase in specific work causes a reduction in the efficiency. The solution of the problem will identify those values of the decision variables that give the best balance between efficiency and specific work.

B. Geometrical and Operational Parameters

To completely define the problem, all unmodified geometrical and operational parameters had to be set. To do this, we used as baseline geometry the test case known in literature as *E/TU-3 (AGARD AR 275)*, i.e. is a subsonic single-stage gas turbine, whose geometrical parameters are listed in Table I. Note that all parameters varying with radius are given referring to their mid-span values. Moreover, rotor blades are unshrouded.

TABLE I
Geometrical Parameters

Parameter	Value
Hub diameter – Stator [mm]	340.0
Hub diameter – Rotor [mm]	335.4
Shroud diameter – Stator [mm]	450.0
Shroud diameter – Rotor [mm]	450.0
Pitch – Stator [mm]	95.5
Pitch – Rotor [mm]	62.8
Number of blades – Stator	20
Number of blades – Rotor	31
Axial distance – Stator/Rotor [mm]	54.0
Inlet stator blade angle [deg]	0
Outlet stator blade angle [deg]	68.9
Inlet rotor blade angle [deg]	47.6
Outlet rotor blade angle [deg]	-57.5
Tip clearance – Stator [mm]	0
Tip clearance – Rotor [mm]	0.25

Regarding operational parameters, as the operating fluid has changed from gas (original fluid) to steam (fluid used for the optimization), thermodynamic parameters were properly modified. More specifically, inlet total temperature and pressure were reset referring to existing steam turbines typically installed in thermoelectric power plants, while the range for corrected mass flow rate was calculated starting from the Kacker & Okapuu diagram. Because of the impossibility to calculate supersonic operating condition using Craig & Cox model, lower and upper limit for mass flow rate range were both set at lower values than the "optimum" mass flow rate suggested by Kacker & Okapuu diagram. This choice does not represent a limitation, as the optimization process will consequently modify the geometry.

Unlike thermodynamic parameters, turbine rotational speed remained unchanged, as independent from the operational fluid used. New operational parameters are listed in Table II.

TABLE II
Operational Parameters

Quantity	Value
Inlet total temperature [K]	733.15
Inlet total pressure [bar]	20
Minimum corrected mass flow rate [(Kg·K$^{0.5}$)/(s·bar)]	35
Maximum corrected mass flow rate [(kg·K$^{0.5}$)/(s·bar)]	47
Corrected mass flow rate step [(kg·K$^{0.5}$)/(s·bar)]	1
Rotational speed [rev/min]	7800

C. Multi-Point Optimization

In turbine optimization it is essential to know whether the machine will operate in a single fixed point or if it will work within a defined range of operating conditions. In the present paper, the latter case was considered which requires a multi-point optimization approach.

This approach operates evaluating objective functions in more than one operating points (e.g. at varying of mass flow rates) and using as "global" objective functions (i.e. those functions used by genetic algorithm) the average of each of the objective functions at varying of mass flow rate.

D. Genetic Algorithm Parameters

Before launching the optimization, other parameters had to be defined. Among them the most relevant were:

- A function to create the initial population: the two main alternatives are either to populate only the borders of the feasible domain or to uniformly populate all the feasible domain. In this optimization, we went for the second option;
- Numbers of individuals produced at each generation. We used 50 individuals, as the minimum number of individuals suggested was between 2n (10 individuals) and 4n (20 individuals), being n the number of decision variables;
- Crossover fraction: determines the fraction of individuals created through crossover of chromosomes taken from the previous generation; the complementary fraction is created through mutation. In this work the crossover fraction was set equal to 7/10;
- Crossover function: determines how the crossover operation is carried out. Hereafter an *intermediate crossover* function was chosen, as it enhanced feasible domain exploration.

IV. Optimization Code Runs and Analysis of Results

In this section, the most relevant results from the optimizations are shown. For each of them, the following parameters had to be properly set: side constraints, specific individuals in the initial population (if present), maximum number of generations, and number of individuals produced at each generation (if different from previously defined value of 50 individuals).

A. First Optimization Run

This first optimization run was performed to investigate code and turbine behavior: for this reason, side constraints were set considering only limitations imposed by Craig & Cox model (i.e. correlations feasible domain, diagrams ranges, etc).

1. Settings

Being this an explorative optimization performed only to identify appropriate side constraint for next optimizations, maximum number of generations was limited to 100; number of individuals created at each generation was set equal to 50; no specific individuals were manually introduced in the first generation to avoid influencing the optimization results. Side constraints were adopted according to Table III.

TABLE III
Side Constraint – First Run

Parameter	Value
Min outlet stator blade angle [deg]	45
Max outlet stator blade angle [deg]	80
Min inlet rotor blade angle [deg]	- 10
Max inlet rotor blade angle [deg]	60
Min outlet rotor blade angle [deg]	- 80
Max outlet rotor blade angle [deg]	- 45
Min stator cascade solidity	0.9
Max stator cascade solidity	2.5
Min rotor cascade solidity	0.9
Max rotor cascade solidity	2.5

Side constraint ranges are hereafter explained:

- All cascade solidity constraints depend on Craig & Cox diagrams limitations;
- Minimum inlet rotor blade angle was set as a consequence of previous calculations showing that, for angle smaller than -10 deg, the degree of reaction became higher than 0.5 (condition known to reduce both efficiency and specific work done in steam turbines);
- Max outlet stator blade angle was set considering that large angles would cause stator outlet section restriction and higher flow deflection. As both phenomena would produce velocity increase, max outlet stator blade angle constraint was set to limit velocity and avoid sonic speed in the throat section;
- Inlet rotor blade angle range was set referring to typical 0.5 degree of reaction geometry (inlet rotor blade angle around 0 deg) and typical low reaction geometry (inlet rotor blade angle approximately equal to outlet rotor blade angle);
- Outlet rotor blade angle range was suggested by previous calculation that identified with $\beta_{2c} \approx$ -67 deg the condition of axial absolute flow at rotor outlet.

Eventually, only for this run, corrected mass flow rate step was reduced to 0.5 [(kg·K$^{0.5}$)/(s·bar)] in order to have higher resolution in plotting maps, making easier to identify numerical problems in the code, if present.

2. Results

Main results of the optimization are shown in the objective functions domain, where the evolution of Pareto front at each generation can be plotted. In Fig. 1 to Fig. 4, Pareto front evolution is presented; in these diagrams x-axis represents the objective function $1-\eta_{ts}$, while y-axis represents the objective function $-L$. Note that alongside each front the corresponding generation number is indicated.

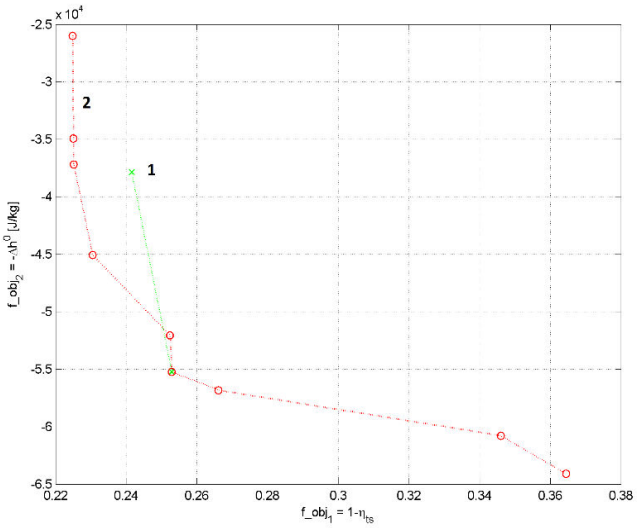

Fig. 1 Pareto front at 1st and 2nd generations – 1st optimization

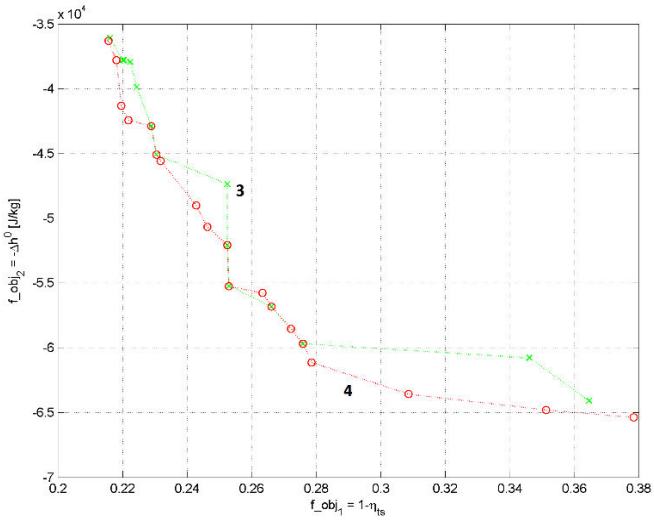

Fig. 2 Pareto front at 3rd and 4th generations – 1st optimization

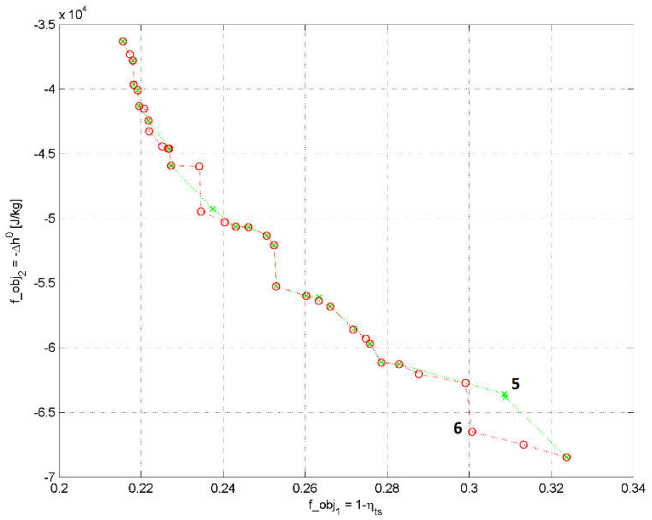

Fig. 3 Pareto front at 5th and 6th generations – 1st optimization

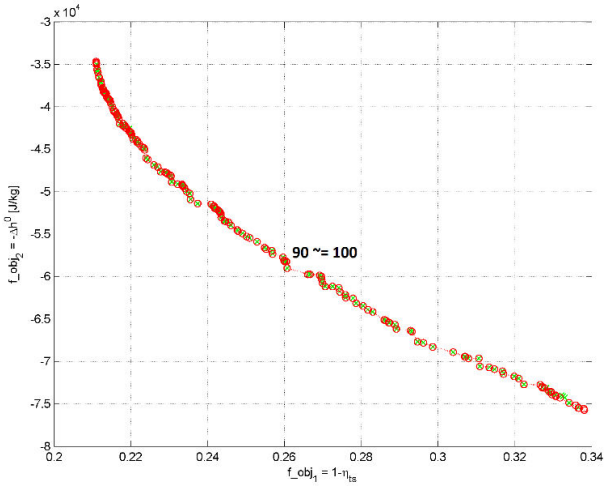

Fig. 4 Pareto front at 90th and 100th generations – 1st optimization

It is clear that Pareto front evolution is more pronounced during the first generations, as the genetic algorithm starts from a casual population and evolves towards populations with higher fitness.

Another relevant information is shown in Fig. 5, where total-to-static efficiency vs. ratio of specific work to inlet total temperature is plotted for the maximum efficiency individual and the maximum specific work individual on the last Pareto front calculated (100th generation).

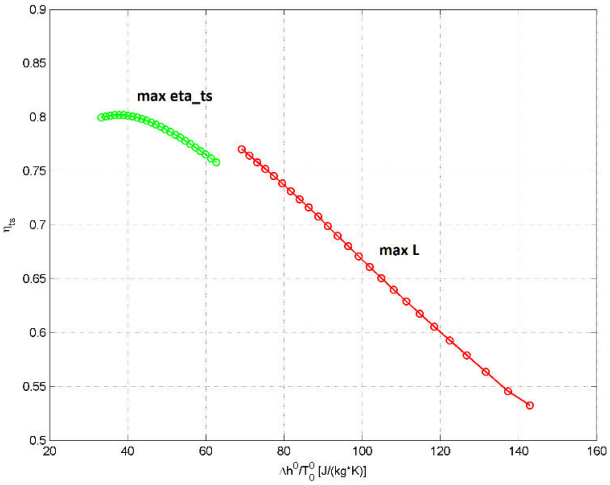

Fig. 5 η_{ts} vs. $\Delta h^0 / T_0^0$ – Maximum η_{ts} and maximum L individuals – Pareto front of last generation – 1st optimization

Each of the plotted points, belonging to a single curve, corresponds to a different value of mass flow rate considered to carry out the desired multi-point optimization. Once again, Fig. 5 confirms that the objective functions chosen represent conflicting targets.

Eventually, other useful diagrams that helped to carry out results analysis were: decision variables vs. generation number (see Fig. 6 to Fig. 10) and objective functions vs. decision variables on the last generation Pareto front (see Fig. 11 to Fig.

15). The first type of diagram suggested new side constraints for the next optimizations, while the second type helped identifying decision variables influence on turbine behavior.

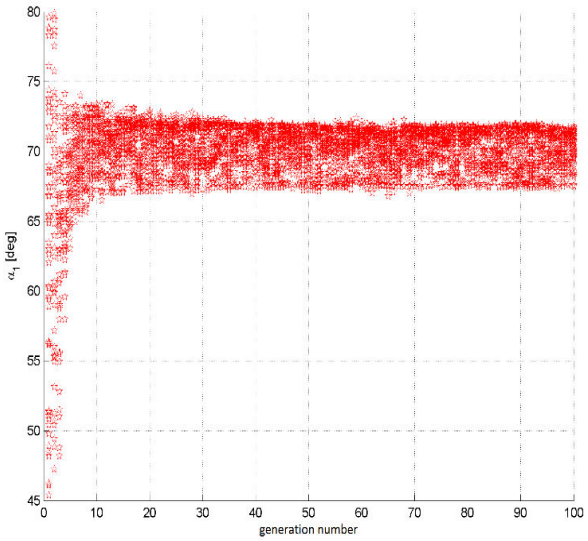

Fig. 6 α_{1c} vs. generation number – 1st optimization

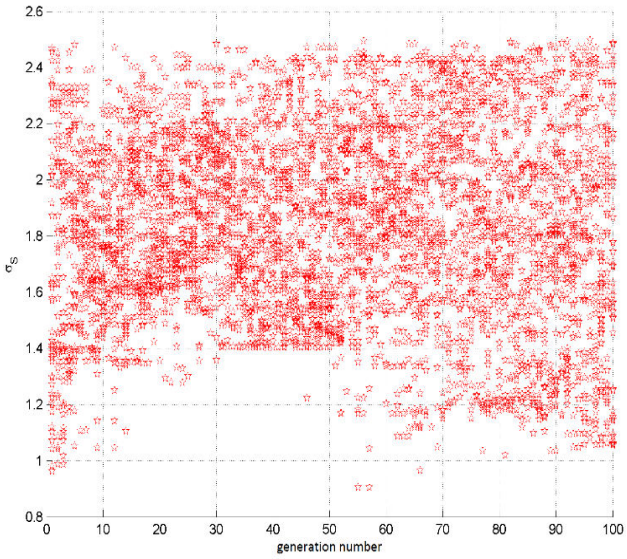

Fig. 7 σ_S vs. generation number – 1st optimization

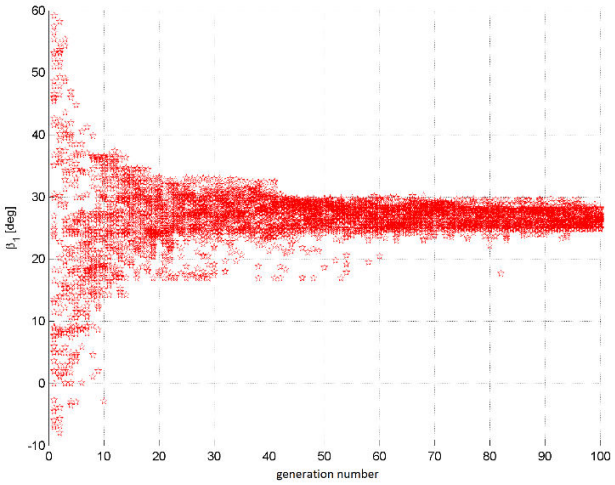

Fig. 8 β_{1c} vs. generation number – 1st optimization

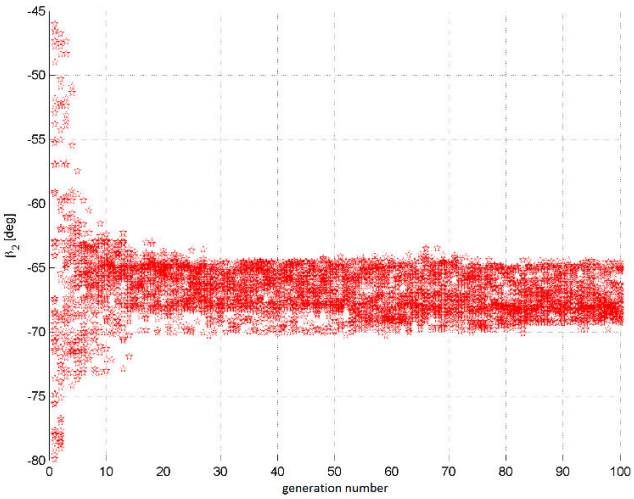

Fig. 9 β_{2c} vs. generation number – 1st optimization

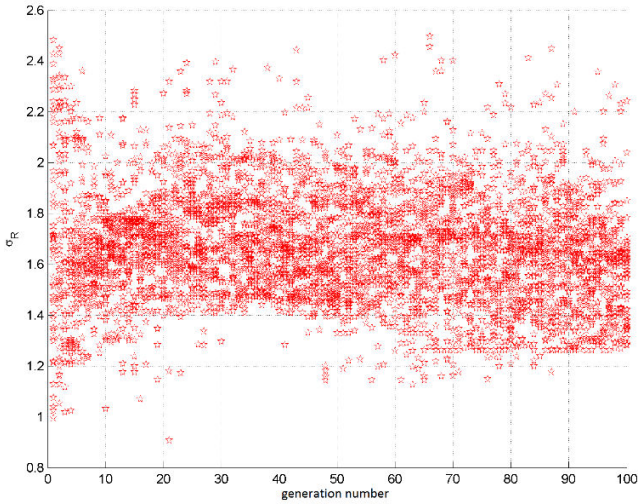

Fig. 10 σ_R vs. generation number – 1st optimization

By observing Fig. 6 to Fig. 10, two different behaviors are shown: while solidities are widely spread over the plotted range of values, angles converge to well defined and restricted ranges. This information will be used to set new side constraint at the beginning of the next optimization.

Fig. 7 reports the effect of mutation operator on decision variables progression: in this specific case, between 30th and 45th generations the minimum value of solidity is around 1.4; shortly after, some new individuals appear having lower values than 1.4. This is a clear effect of the mutation operator, as it produced individuals located outside the range of values characterizing previous generations. Note that the new individuals manage to survive and reproduce, getting even to the last generation.

As mentioned above, other useful information can be obtained by studying Fig. 11 to Fig. 15, where efficiency vs. decision variables diagrams is plotted.

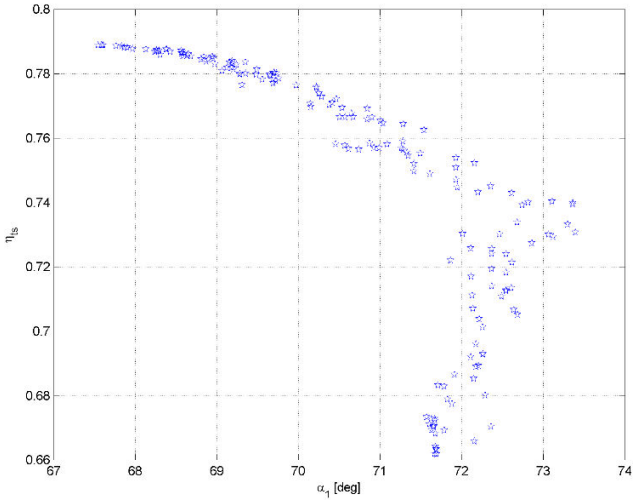

Fig. 11 η_{ts} vs. α_{1c} – last Pareto front – 1st optimization

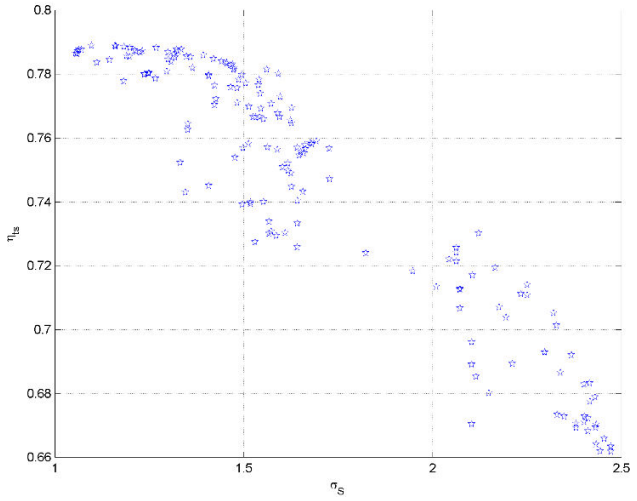

Fig. 12 η_{ts} vs. σ_S – last Pareto front – 1st optimization

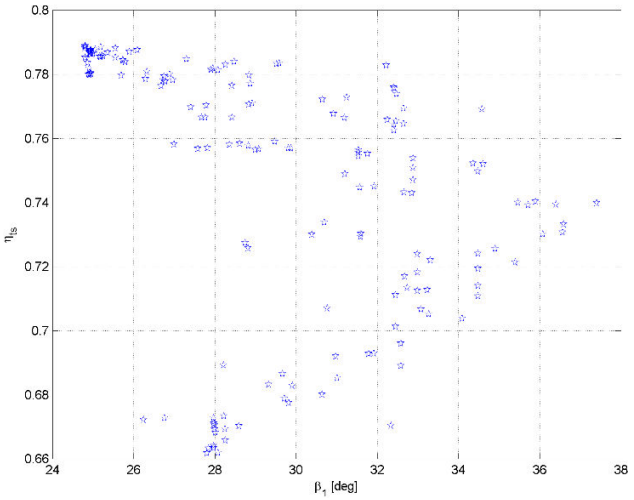

Fig. 13 η_{ts} vs. β_{1c} – last Pareto front – 1st optimization

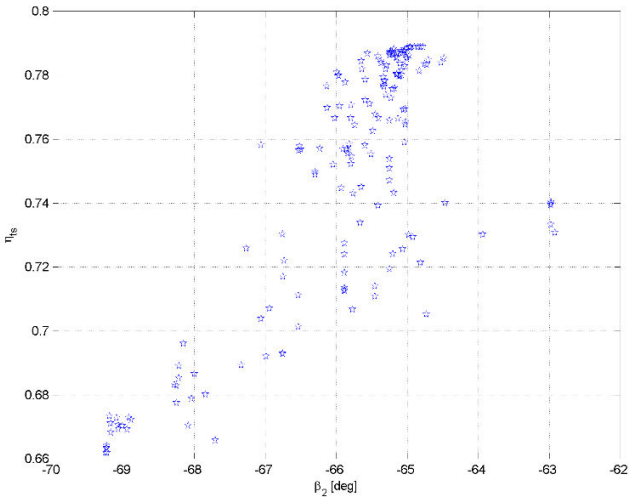

Fig. 14 η_{ts} vs. β_{2c} – last Pareto front – 1st optimization

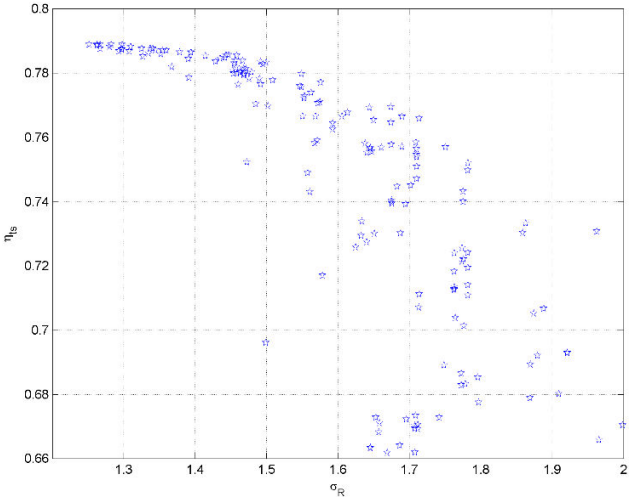

Fig. 15 η_{ts} vs. σ_R – last Pareto front – 1st optimization

While points plotted in Fig. 13 and Fig. 15 are widely scattered, the examination Fig. 11, Fig. 12, and Fig. 14 can give useful information about turbine operation.

Starting from individuals with the highest efficiency and moving toward low efficiency values (i.e. high specific work values), both α_{1c} and σ_S progressively increase, causing higher flow deflection in the stator cascade, which means growing values for c_{u1}. Simultaneously, β_{2c} angle remains constant and equal to the value which gives almost axial absolute velocity at rotor outlet, thus limiting kinetic energy losses at turbine outlet.

Reaching values of $\eta_{ts} < 0.73$, a new phenomenon comes up: α_{1c} cannot increase its value anymore and, at the same time, β_{2c} angle starts decreasing. This behavior can be explained remembering that Craig & Cox model cannot calculate sonic conditions; because of this, the optimization code was programmed to exclude all individuals producing sonic or supersonic conditions either at stator or at rotor outlet. In fact, both increase of α_{1c} and of σ_S cause reduction of stator outlet section, and increase in flow deflection through stator cascade, that is an unremitting increase of speed at stator outlet. For this reason, once sonic speed is reached at stator outlet, α_{1c} is not allowed to increase anymore; in this situation, the only way to increase furthermore specific work done, despite of efficiency reduction, is to investigate higher deflection in the rotor cascade by increasing $|\beta_{2c}|$, which means by increasing $|c_{u2}|$ (remember that specific work can be expressed as in (1)). Fig. 14 confirms this explanation.

B. Second Optimization Run

The second optimization was configured considering previously obtained results. Side constraints were set accordingly with decision variables evolutions shown in Fig. 6 to 10 paying particular attention to the sonic problem already encountered, but without unwisely limiting the decision variables domain.

1. Settings

Unlike the first run, with this optimization we aimed to find the Pareto-optimal front of the considered problem. For this reason the maximum number of generation was increased to 250, while keeping the number of individuals at each generation equals to 50. No individuals were manually introduced in the starting population, to allow a free evolution starting from a completely casual population. Side constraints were set as listed in Table IV.

TABLE IV
SIDE CONSTRAINT – SECOND RUN

Parameter	Value
Min outlet stator blade angle [deg]	45
Max outlet stator blade angle [deg]	72.5
Min inlet rotor blade angle [deg]	- 10
Max inlet rotor blade angle [deg]	60
Min outlet rotor blade angle [deg]	- 72.5
Max outlet rotor blade angle [deg]	- 45
Min stator cascade solidity	0.9
Max stator cascade solidity	2.5
Min rotor cascade solidity	0.9
Max rotor cascade solidity	2.5

Note that multi-point optimization was performed adopting a 1 [(kg·K$^{0.5}$)/(s·bar)] step for corrected mass flow rate.

2. Results

First, to analyze optimization results Pareto fronts evolution was studied and compared to previous results (see Fig. 16 to Fig. 20). Note that alongside each front the corresponding generation number is indicated.

As before, Pareto front moves faster during the first generations, as initial population is still randomly generated. On the other hand, it is important to observe that also during last generations improvements take place (see Fig. 20), but are inevitably slower.

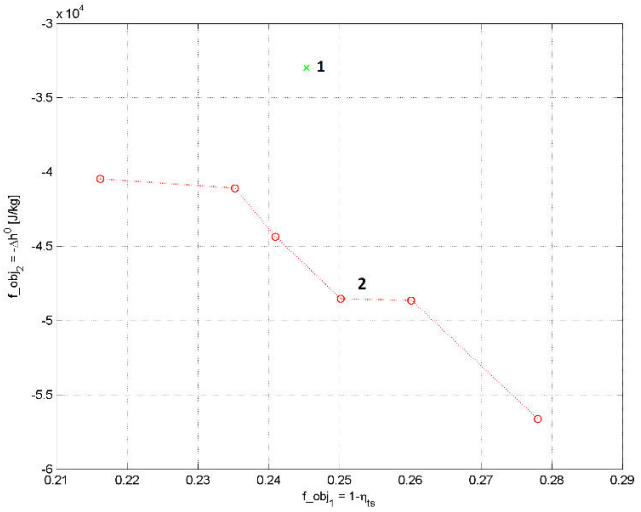

Fig. 16 Pareto front at 1st and 2nd generations – 2nd optimization

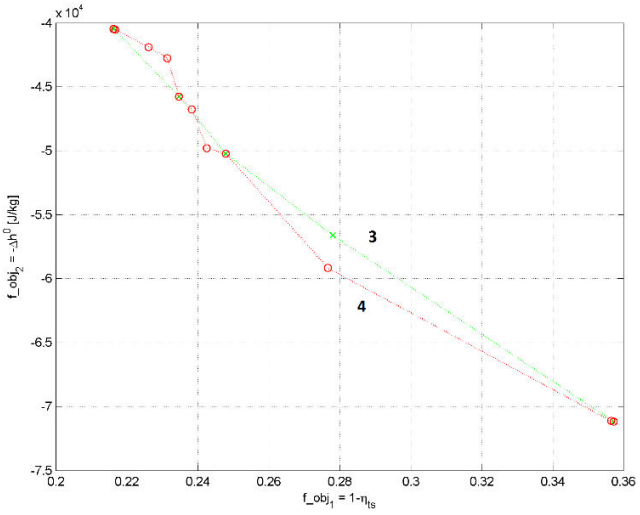

Fig. 17 Pareto front at 3rd and 4th generations – 2nd optimization

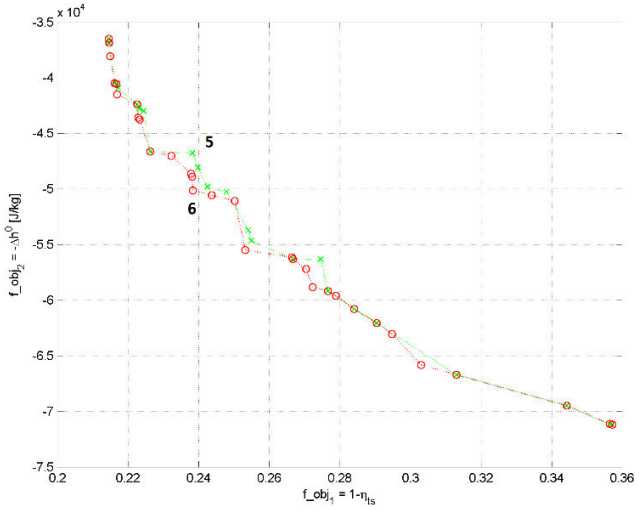

Fig. 18 Pareto front at 5th and 6th generations – 2nd optimization

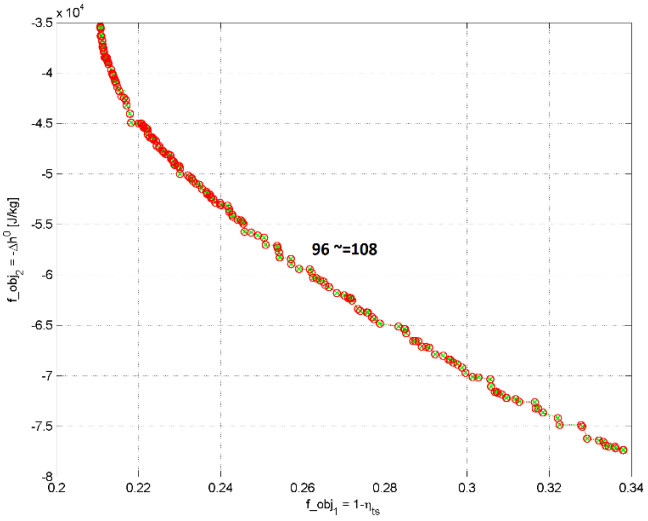

Fig. 19 Pareto front at 96th and 108th generations – 2nd optimization

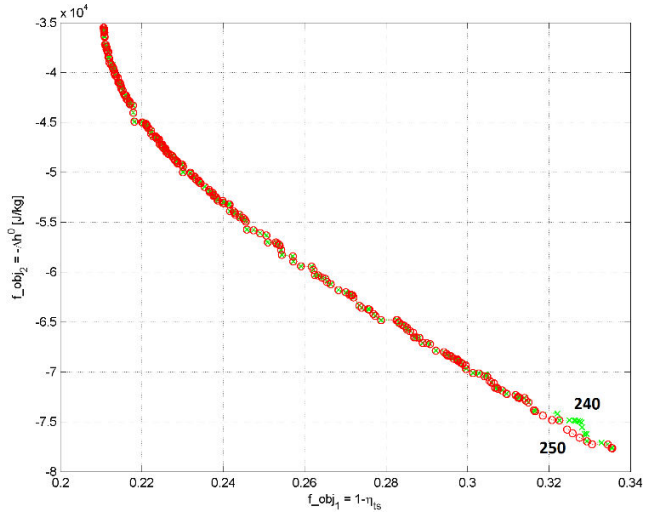

Fig. 20 Pareto front at 240th and 250th generations – 2nd optimization

As can be seen by comparing Fig. 20 and Fig. 4, the Pareto front now obtained for the last generation is slightly shifted downward. This means that the solutions given by the second optimization provide higher values of specific work without reduction of efficiency; this is likely to be caused by the larger number of generations calculated in this second optimization.

Referring to the Pareto front of the 250th generation, Fig. 21 shows total-to-static efficiency vs. ratio on specific work to inlet total temperature both for maximum efficiency and for maximum specific work individuals. By comparing Fig. 21 and Fig. 5, it is confirmed what observed above: the current optimization has identified geometries capable of giving higher value of specific work, without any reduction in maximum efficiency.

Once again, other diagrams used to carry out results analysis were: decision variables vs. generation number (see Fig. 22 to Fig. 26) and objective functions vs. decision variables on the last generation Pareto front (see Fig. 27, Fig. 11 to Fig. 31).

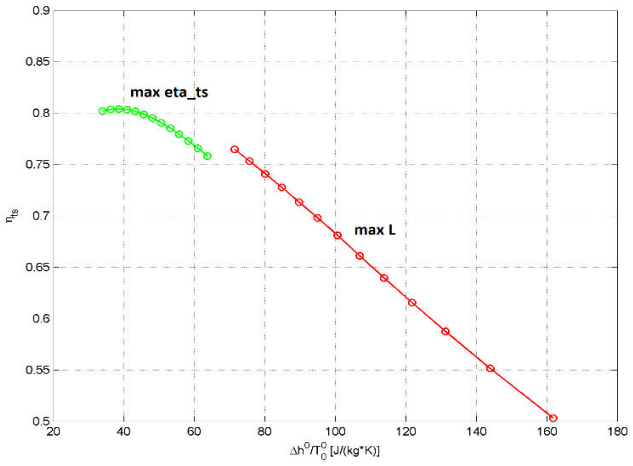

Fig. 21 η_{ts} vs. $\Delta h^0 / T_0^0$ – Maximum η_{ts} and maximum L individuals – Pareto front of last generation – 2nd optimization

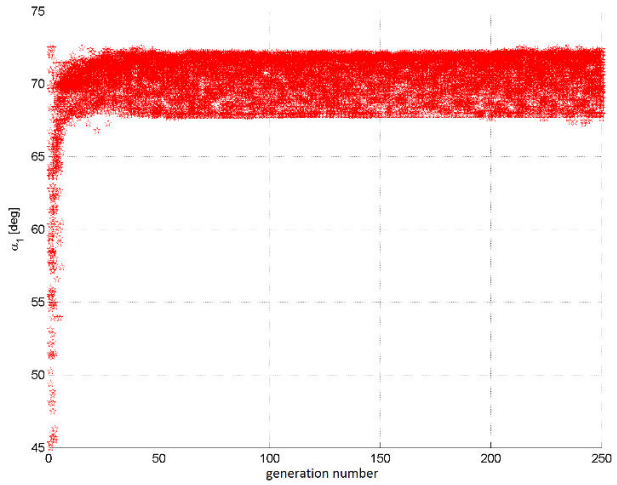

Fig. 22 α_{1c} vs. generation number – 2nd optimization

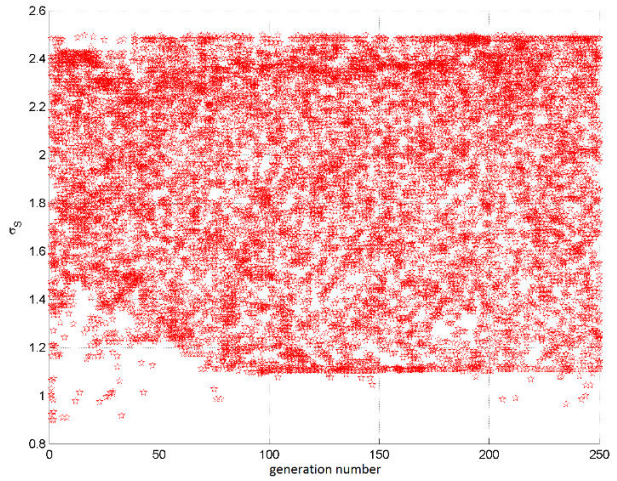

Fig. 23 σ_S vs. generation number – 2nd optimization

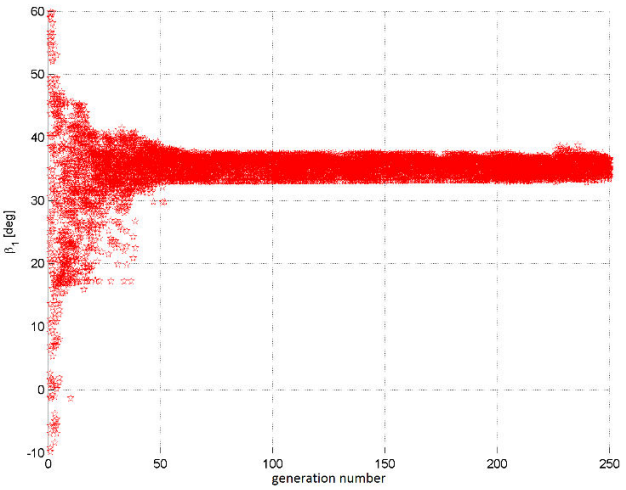

Fig. 24 β_{1c} vs. generation number – 2nd optimization

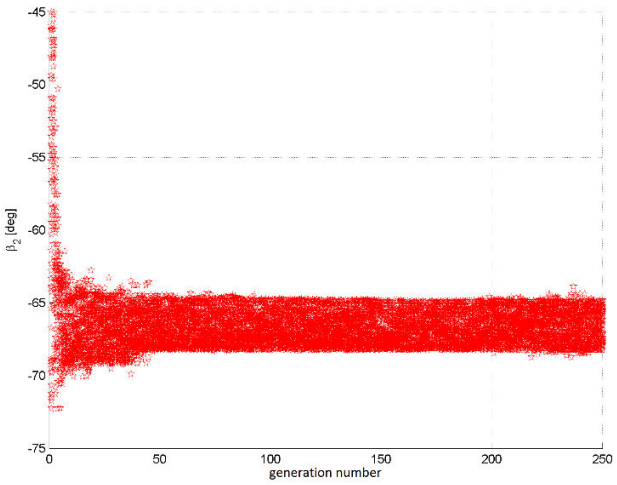

Fig. 25 β_{2c} vs. generation number – 2nd optimization

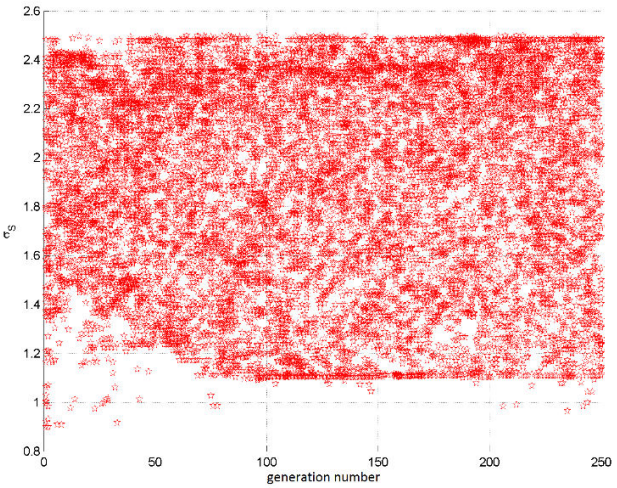

Fig. 26 σ_R vs. generation number – 2nd optimization

Fig. 22 to 26 are in good agreement with what already observed in the previous optimization, with the only exception of the convergence range of values for β_{1c} (see Fig. 8 and 24). This fact is probably attributable both to different degree of convergence and to different side constraint for the problem.

Eventually, objective functions vs. decision variables diagrams were plotted to study whether modified side constraints had solved the problem of sonic condition at stator outlet or not (see Fig. 27 to31). In these diagrams, points are distributed much more regularly than those obtained in the previous optimization: while before for $\eta_{ts} \simeq 0.73$ distribution discontinuities were present (see Fig. 11 and Fig. 12), now decision variables vary almost continuously.

The obtained results confirm that changes applied to side constraint values were correct and solved the sonic problem. This information was used to set up the third and conclusive optimization.

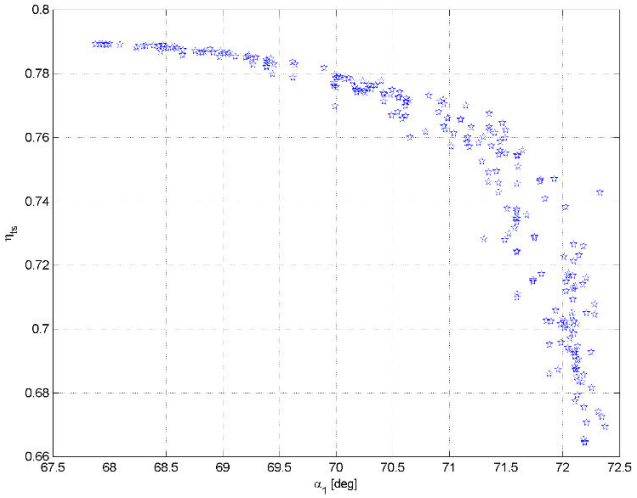

Fig. 27 η_{ts} vs. α_{1c} – last Pareto front – 2nd optimization

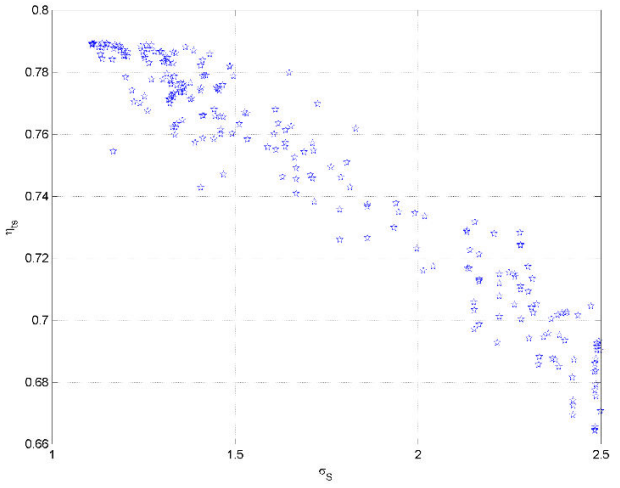

Fig. 28 η_{ts} vs. σ_S – last Pareto front – 2nd optimization

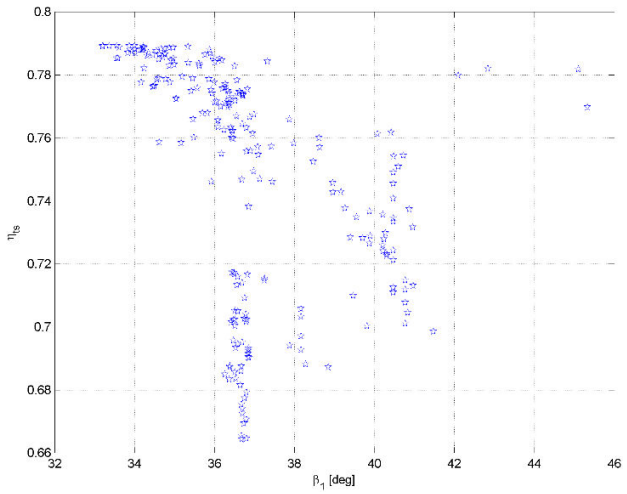

Fig. 29 η_{ts} vs. β_{1c} – last Pareto front – 2nd optimization

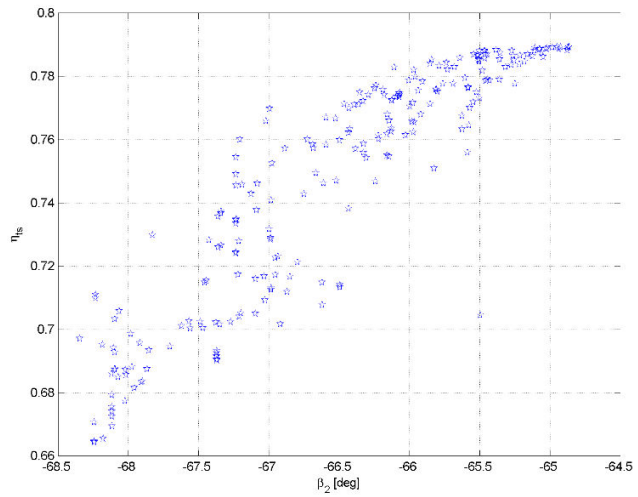

Fig. 30 η_{ts} vs. β_{2c} – last Pareto front – 2nd optimization

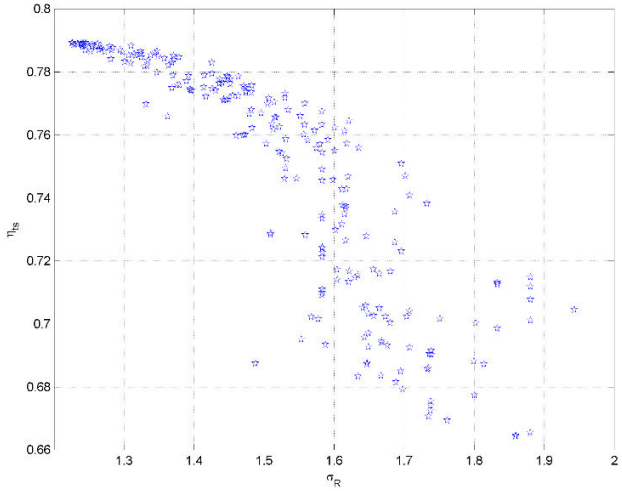

Fig. 31 η_{ts} vs. σ_R – last Pareto front – 2nd optimization

C. Third Optimization Run

The third and last optimization was performed to identify the real Pareto front of our problem. Being the conclusive optimization, a more accurate results analysis was carried out.

1. Settings

To facilitate the maximum improvement of the Pareto front, the following settings were adopted: maximum number of generations increased to 300; completely free initial population; number of individuals at each generation equal to 50; step for corrected mass flow rate equals to 1 [(kg·K$^{0.5}$)/(s·bar)]. Eventually, side constraints were set as listed in Table V (slightly modified from values used for the second run).

TABLE V
SIDE CONSTRAINT – THIRD RUN

Parameter	Value
Min outlet stator blade angle [deg]	45
Max outlet stator blade angle [deg]	72
Min inlet rotor blade angle [deg]	- 10
Max inlet rotor blade angle [deg]	60
Min outlet rotor blade angle [deg]	- 72
Max outlet rotor blade angle [deg]	- 45
Min stator cascade solidity	0.9
Max stator cascade solidity	2.5
Min rotor cascade solidity	0.9
Max rotor cascade solidity	2.5

2. Results

The Pareto front evolution is comparable to the one observed during the previous optimization; because of this, only the last Pareto fronts was be plotted (see Fig. 32; alongside each front is indicated the corresponding generation number). Note that Fig. 20 and 32 are virtually identical which means that no improvement was obtained by simply increasing the number of generations. This fact suggested that the Pareto front found both by the second and by the third optimizations was the real Pareto front for our problem. This hypothesis will be further investigated hereafter.

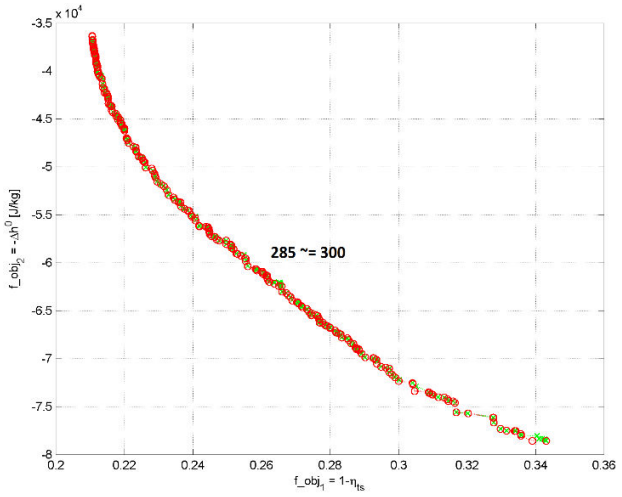

Fig. 32 Pareto front at 285th and 300th generations – 3rd optimization

Now, as both decision variables vs. generation number diagrams and objective functions vs. decision variables diagrams were very similar to those obtained previously, in this case we focused on turbine maps for three individuals chosen on the last Pareto front: the first individual with maximum efficiency (see Fig. 33 and 34), the second with a balance of efficiency and specific work efficiency (see Fig. 35 and Fig. 36), and the third with maximum specific work done (see Fig. 37 and Fig. 38).

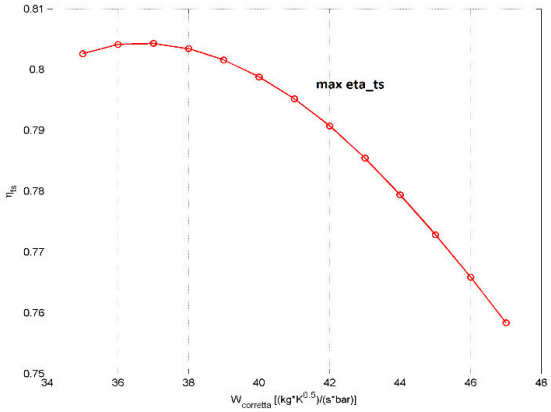

Fig. 33 η_{ts} vs. corrected mass flow rate – maximum efficiency individual – 3rd optimization

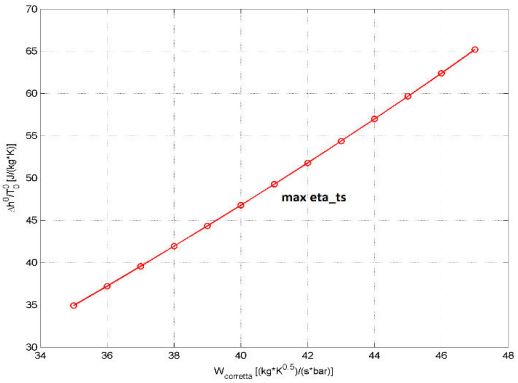

Fig. 34 Ratio of L to inlet total temperature vs. corrected mass flow rate – maximum efficiency individual – 3rd optimization

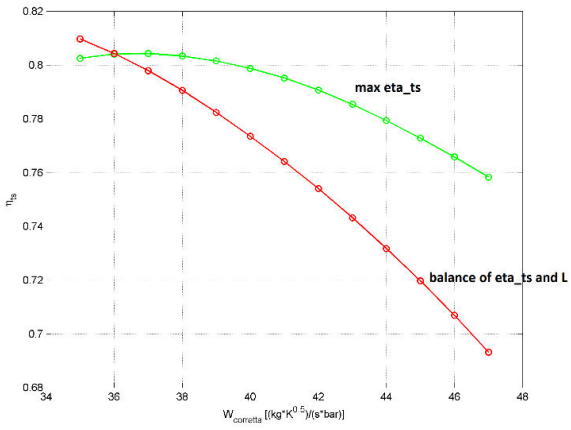

Fig. 35 η_{ts} vs. corrected mass flow rate – maximum efficiency, and balanced individuals – 3rd optimization

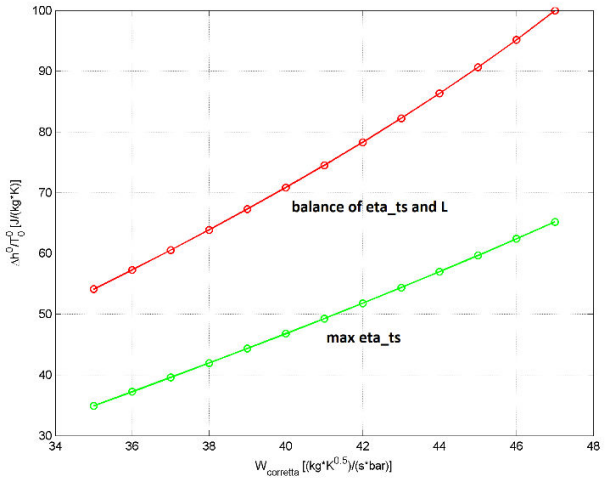

Fig. 36 Ratio of L to inlet total temperature vs. corrected mass flow rate – maximum efficiency, and balanced individual

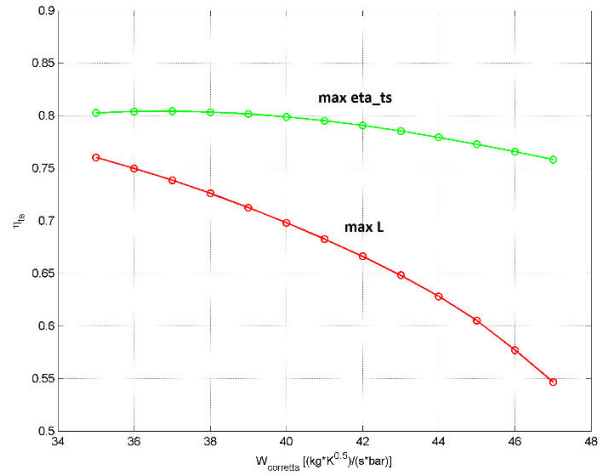

Fig. 37 η_{ts} vs. corrected mass flow rate – maximum efficiency, and maximum specific work individuals

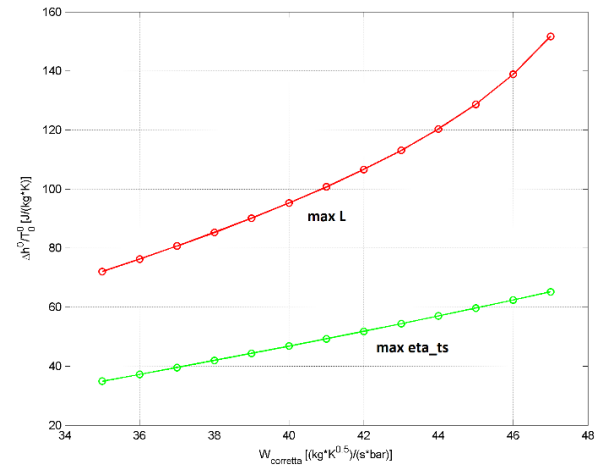

Fig. 38 Ratio of L to inlet total temperature vs. corrected mass flow rate – maximum efficiency, and maximum specific work individuals

For the three representative individuals considered above (to plot the turbine maps), corresponding decision variables values are listed in Table VI.

TABLE VI
DECISION VARIABLE VALUES – MOST SIGNIFICANT INDIVIDUALS

Variable	Max η_{ts} individual	Balanced individual	Max L individual
α_{1c} [deg]	68.241	71.692	71.893
σ_S	1.1197	1.4077	2.448
β_{1c} [deg]	37.971	46.141	48.678
β_{2c} [deg]	- 64.812	- 66.792	- 68.753
σ_R	1.2274	1.5139	2.0807

At this point we verified that the obtained results and decision variables, even if generated exclusively by the genetic algorithm, agreed with fluid dynamic considerations. Starting from the individual having higher efficiency, moving toward the individual giving the higher specific work we observed that:

1. α_{1c} value increases. This is reasonable as it is associated with an increase in c_{u1} and, through (1), with an increase in L. At the same time, higher deflection causes reduction of efficiency.
2. σ_S value increases. This is reasonable too, as variations in σ_S has similar effect to variations in α_{1c}.
3. β_{1c} value increases. This is due to stator-rotor coupling: to avoid bad incidence at rotor inlet, when α_{1c} value increase, β_{1c} value must increase too.
4. $|\beta_{2c}|$ value increases. This is reasonable as we know that maximum efficiency individual has almost axial absolute flow at rotor outlet, which means that increases in $|\beta_{2c}|$ value cause increases in $|c_{u2}|$ value, that means higher L, but lower efficiency.
5. σ_R value increases. This can be explained in the same way of σ_S value increase.

This means that the obtained results are consistent with fluid dynamic phenomena.

To complete this analysis, we eventually verified that the Pareto front obtained at the 300th generation was really the Pareto-optimal front of our problem. This operation was carried out by launching three local optimizations: the first one around the maximum efficiency individual, the second one around the balanced individual, and the third one around the maximum specific work individual. To modify the explored domain in each of the three cases, we manually introduced in the initial population individuals belonging to the considered Pareto front; moreover, we properly modified side constraint. Eventually, being local optimization, the maximum number of

generations was limited to 50.

Hereafter side constraints adopted are listed (Tables VII-IX) and the corresponding Pareto fronts obtained, together with the manually introduced initial individuals (Fig. 39-Fig. 41).

TABLE VII
SIDE CONSTRAINT – FIRST LOCAL RUN – MAXIMUM EFFICIENCY

Parameter	Value
Min outlet stator blade angle [deg]	67
Max outlet stator blade angle [deg]	71
Min inlet rotor blade angle [deg]	25
Max inlet rotor blade angle [deg]	46
Min outlet rotor blade angle [deg]	- 67
Max outlet rotor blade angle [deg]	- 64.5
Min stator cascade solidity	1
Max stator cascade solidity	1.75
Min rotor cascade solidity	1.15
Max rotor cascade solidity	1.5

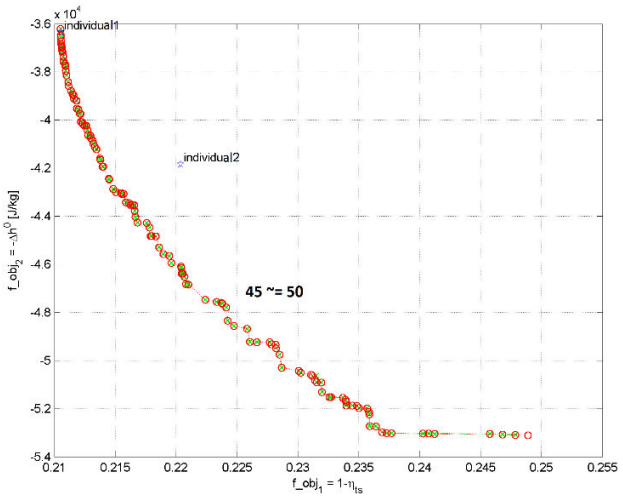

Fig. 39 Pareto front at 45th and 50th generations – 1st local optimization (maximum efficiency)

TABLE VIII
SIDE CONSTRAINT – SECOND LOCAL RUN – BALANCED

Parameter	Value
Min outlet stator blade angle [deg]	70
Max outlet stator blade angle [deg]	71.5
Min inlet rotor blade angle [deg]	30
Max inlet rotor blade angle [deg]	48
Min outlet rotor blade angle [deg]	- 67.5
Max outlet rotor blade angle [deg]	- 65
Min stator cascade solidity	1.25
Max stator cascade solidity	1.75
Min rotor cascade solidity	1.4
Max rotor cascade solidity	1.7

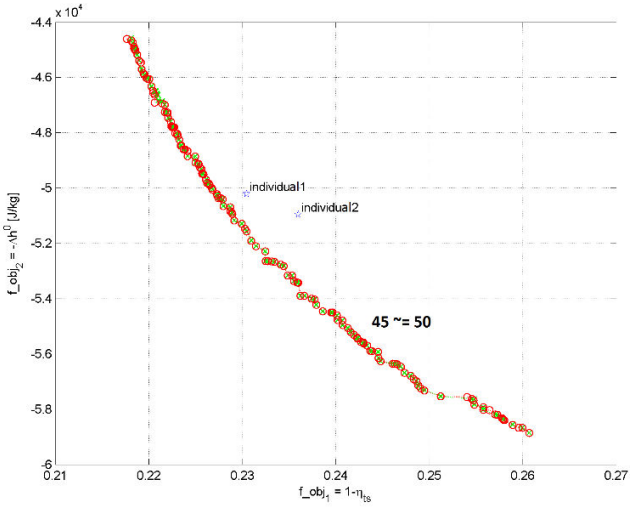

Fig. 40 Pareto front at 45th and 50th generations – 2nd local optimization (balanced performance)

TABLE IX
SIDE CONSTRAINT – THIRD LOCAL RUN – MAXIMUM SPECIFIC WORK

Parameter	Value
Min outlet stator blade angle [deg]	71
Max outlet stator blade angle [deg]	75
Min inlet rotor blade angle [deg]	36
Max inlet rotor blade angle [deg]	52
Min outlet rotor blade angle [deg]	- 72
Max outlet rotor blade angle [deg]	- 65
Min stator cascade solidity	2
Max stator cascade solidity	2.5
Min rotor cascade solidity	0.9
Max rotor cascade solidity	2.5

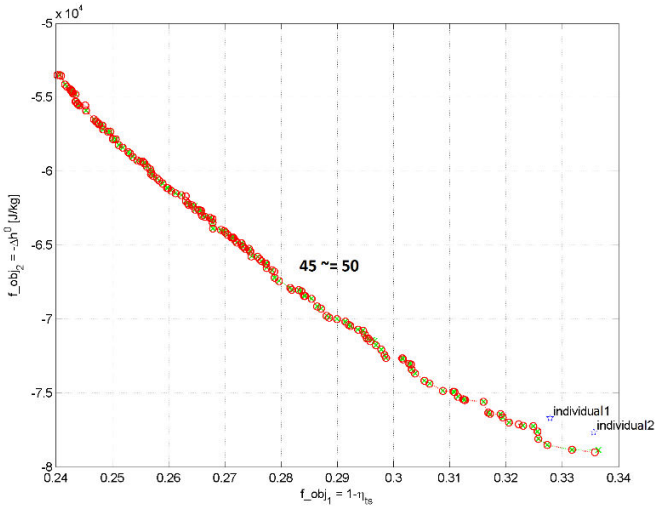

Fig. 41 Pareto front at 45th and 50th generations – 3rd local optimization (maximum specific work)

Looking at numerical values, it is clear that this local optimization did not manage to significantly reduce objective functions values. This eventually suggested that the Pareto front obtained at the 300th generation of the 3rd global optimization could be considered as the real Pareto-optimal

front for our problem.

V. Conclusions

The results were presented of a study of the suitability of optimization algorithms to steam turbine design. The code developed proved its ability to identify the Pareto-optimal solutions, providing the best balance of total-to-static efficiency and specific work done. In fact, geometrical parameters generated by the optimization approach were in perfect agreement with fluid dynamic considerations.

Moreover, the study emphasized the relevance of side constraints values in influencing the degree of convergence attainable by the solution.

This said the developed code is an excellent starting point to carry out an optimized turbine design: due to extremely fast objective functions evaluation, it can explore wide decision variables domains, managing to locate the region giving Pareto-optimal individuals. At the same time, it is important to keep in mind that even modern algebraic one-dimensional losses and deviation models can be slightly inaccurate; for this reason one-dimensional optimization must always be followed by CFD simulations either to confirm or to revise previously obtained results.

Eventually, this code can be easily modified to change both decision variables and objective functions in type and numbers; moreover, a stage stacking option can be introduced, allowing to optimize not only individual turbine stages but also entire multi-stage turbines.

References

[1] Singiresu S. Rao, *Engineering Optimization: Theory and Practice*, 2009, John Wiley & Sons, Inc., Hoboken, New Jersey

[2] E. Benini, G. Boscolo, A. Garavello, 2008, *Assessment of loss correlations for performance prediction of low reaction gas turbine stages*, Proceedings of the ASME International Mechanical Engineering Congress and Exposition, IMECE08, Boston, Massachusetts, USA, IMECE2008-69085, 2008

[3] D. G. Ainley and. G. C. R. Mathieson, 1951, *A Method of Performance Estimation for Axial-Flow Turbines*, A.R.C. R.&M. No. 2974, Great Britain

[4] H. R. M. Craig and H. J. A. Cox, 1971, *Performance estimation of axial flow turbines*, Proceedings Institution of Mechanical Engineers, 1970-1971, v. 185, 32/71, Great Britain

[5] Sandrolini Sandro and Naldi Giovanni, *Macchine 2: Le turbomacchine motrici e operatrici*, 1996, Pitagora editrice, Bologna (ITA), ISBN: 88-371-0827-3.